

# Data taking strategy for $\psi(3770)$ and $\Upsilon(4S)$ branching fraction measurements at $e^+e^-$ colliders

Jiixin Li,<sup>1,2</sup> Xiantao Hou,<sup>3,4</sup> Junli Ma,<sup>3,4</sup> Changzheng Yuan,<sup>3,4</sup> and Xiaolong Wang<sup>1,2,\*</sup>

<sup>1</sup>*Key Laboratory of Nuclear Physics and Ion-beam Application, Ministry of Education, China*

<sup>2</sup>*Institute of Modern Physics, Fudan University, Shanghai 200443, China*

<sup>3</sup>*University of Chinese Academy of Sciences,  
19A Yuquan Road, Beijing, 10049, China*

<sup>4</sup>*Institute of High Energy Physics, Chinese Academy of Sciences,  
19B Yuquan Road, Beijing, 10049, China*

## Abstract

The  $\psi(3770)$  and  $\Upsilon(4S)$  states predominantly decay into open-flavor meson pairs, while the decays of  $\psi(3770) \rightarrow \text{non-}D\bar{D}$  and  $\Upsilon(4S) \rightarrow \text{non-}B\bar{B}$  are rare but crucial for elucidating the inner structure and decay dynamics of heavy quarkonium states. To achieve precise branching fraction measurements for the  $\psi(3770) \rightarrow \text{non-}D\bar{D}$  and  $\Upsilon(4S) \rightarrow \text{non-}B\bar{B}$  decays at the high luminosity  $e^+e^-$  annihilation experiments, we employed Monte Carlo simulations and Fisher information to evaluate various data taking scenarios, ultimately determining the optimal scheme. The consistent results of both methodologies indicate that the optimal energy points for  $\psi(3770) \rightarrow \text{non-}D\bar{D}$  decays are 3.769 GeV and 3.781 GeV, while those for  $\Upsilon(4S) \rightarrow \text{non-}B\bar{B}$  decays are 10.574 GeV and 10.585 GeV. In addition, we provide an analysis of the relationship between the integrated luminosity and the precision in branching fraction measurements derived from these data samples, with the branching fraction spanning several orders of magnitude.

---

\* Contact author: [xiaolong@fudan.edu.cn](mailto:xiaolong@fudan.edu.cn)

## I. INTRODUCTION

The  $\psi(3770)$  above the  $D\bar{D}$  threshold and the  $\Upsilon(4S)$  above the  $B\bar{B}$  threshold are two typical broad resonances. Their dominant decay modes are open-flavor meson pair final states and hadronic or radiative transitions to low lying quarkonia. Their decays into light hadronic (non- $D\bar{D}$ , non- $B\bar{B}$ ) final states are suppressed according to the OZI rule [1] and consequently having small branching fractions, i.e.,  $(7_{-8}^{+9})\%$  for the  $\psi(3770)$  and  $< 4\%$  at the 95% confidence level for the  $\Upsilon(4S)$  [2]. According to the available searches from previous experiments, we have good reason to believe that the exact branching fractions to light hadrons should be at 1% level for both  $\psi(3770)$  and  $\Upsilon(4S)$  [3–11]. Most of these studies were performed at  $e^+e^-$  collision experiments, and the total cross sections of the resonance production and continuum process are of the same order of magnitude. In this case, the interference between the continuum and resonance amplitudes might be large and can not be ignored. Mishandling of the interference effect will lead to systematic bias with a much larger size compared with the statistical uncertainty and comparable to or even larger size than all the other sources of systematic uncertainties [12]. The optimal solution to this problem is to change the data taking strategy of accumulating data at the resonance peak and energy points off the peak (called continuum data).

The BESIII and Belle II are  $e^+e^-$  collision experiments in operation at the charmonium and bottomonium energy regions. At the BESIII experiment, 20  $\text{fb}^{-1}$  data have been accumulated by 2024 at the center-of-mass energy  $\sqrt{s} = 3.773$  GeV, which is the peak of the  $\psi(3770)$  [13]. This data sample is at least six times larger than the one collected by BESIII up to 2019 and dozens of times larger than those in the CLEOc and BESII measurements [2]. Belle II experiment plans to take about 50  $\text{ab}^{-1}$  data at the peak of the  $\Upsilon(4S)$  ( $\sqrt{s} = 10.58$  GeV) [14], which are  $10^2$  ( $10^3$ ) of times larger than the data samples of the Belle and BaBar (CLEO) experiments [2]. With the currently available BESIII data sample and the expected Belle II data sample, the precision of the branching fraction of  $\psi(3770) \rightarrow \text{non-}D\bar{D}$  and  $\Upsilon(4S) \rightarrow \text{non-}B\bar{B}$  decays can be improved significantly. Therefore, it is essential to determine the optimal data taken strategy.

This work focuses on the relative uncertainties of the branching fractions of  $\psi(3770) \rightarrow \text{non-}D\bar{D}$  and  $\Upsilon(4S) \rightarrow \text{non-}B\bar{B}$  decays. We take the optimization of  $\psi(3770)/\Upsilon(4S) \rightarrow \eta'\phi$  measurement as an example. Monte Carlo (MC) simulation and Fisher information are employed to simulate various data taking cases with two parameters: the branching fraction of non- $D\bar{D}$  or non- $B\bar{B}$  decays denoted as  $\mathcal{B}$ , and the relative angle between resonance and continuum amplitudes denoted as  $\phi$ . The optimal data taking scheme obtained from both methods is consistent. Herein to achieve the measurements of branching fractions of  $\psi(3770) \rightarrow \text{non-}D\bar{D}$  and  $\Upsilon(4S) \rightarrow \text{non-}B\bar{B}$  decays, we want to figure out:

- What are the optimal  $\sqrt{s}$  values for the data taking around the resonances?
- How many energy points around an optimal  $\sqrt{s}$  are necessary for the scan?
- What are the required data sizes to achieve a specific precision in the branching fraction measurements?

## II. MC SIMULATION METHODOLOGY

### A. Theoretical Framework

Within a specified period of data taking time or equivalently for a given integrated luminosity, we try to find out the scheme that can provide the best precision for branching fraction measurements of  $\psi(3770) \rightarrow \text{non-}D\bar{D}$  or  $\Upsilon(4S) \rightarrow \text{non-}B\bar{B}$  decays. The sampling technique is utilized to simulate various data taking strategies, the optimal of which will be chosen. For specific simulations, the likelihood function is constructed as

$$LF = \prod_{i=1}^{N_{pt}} \frac{1}{\sqrt{2\pi x_i^{\text{exp}}}} e^{-\frac{(x_i - x_i^{\text{exp}})^2}{2x_i^{\text{exp}}}}, \quad (\text{II.1})$$

where  $x_i$  and  $x_i^{\text{exp}}$  are the number of observed events and the one of expected events of  $\psi(3770) \rightarrow \text{non-}D\bar{D}$  or  $\Upsilon(4S) \rightarrow \text{non-}B\bar{B}$  decays, the subscript  $i$  labels the  $i$ -th scan energy point, and  $N_{pt}$  is the number of the energy points. For a certain exclusive final state  $f$ , the  $x_i^{\text{exp}}$  in a data sample taken at the  $i$ -th energy point with an integrated luminosity of  $\mathcal{L}_i$  is given by

$$x_i^{\text{exp}}(\mathcal{B}, \phi) = \mathcal{L}_i \cdot \sigma_{\text{exp}}(\mathcal{B}, \phi, \sqrt{s}) \cdot \epsilon, \quad (\text{II.2})$$

where  $\epsilon$  is the selection efficiency of signal reconstruction, and  $\sigma_{\text{exp}}$  with  $\mathcal{B}$  and  $\phi$  as two parameters is the expected cross section at  $\sqrt{s}$ . The maximum value of  $\mathcal{B}$ , derived from a conservative estimate of the summed branching ratios for the resonance decaying to light hadronic final states as reported by the Particle Data Group (PDG) [2], is  $1 \times 10^{-3}$  for  $\psi(3770) \rightarrow \text{non-}D\bar{D}$  decays and  $1 \times 10^{-6}$  for  $\Upsilon(4S) \rightarrow \text{non-}B\bar{B}$  decays. The cross section  $\sigma_{\text{exp}}$  can be written as

$$\sigma_{\text{exp}}(\sqrt{s}) = |a_c^f(\sqrt{s}) + e^{i\phi} \cdot a_R^f(\sqrt{s})|^2, \quad (\text{II.3})$$

where  $a_c^f(\sqrt{s})$  is the continuum amplitude of  $e^+e^- \rightarrow f$  and  $a_R^f(\sqrt{s})$  is the resonance amplitude of  $R \rightarrow f$ . They are parametrized as

$$a_c^f(\sqrt{s}) = \frac{a}{(\sqrt{s})^n} \sqrt{PS(\sqrt{s})}, \quad (\text{II.4})$$

$$a_R^f(\sqrt{s}) = \frac{\sqrt{12\pi\Gamma_{e^+e^-}\Gamma\mathcal{B}}}{s - M^2 + iM\Gamma} \sqrt{\frac{PS(\sqrt{s})}{PS(M)}}, \quad (\text{II.5})$$

where  $PS(\sqrt{s})$  is the phase space factor at  $\sqrt{s}$ . In the continuum amplitude, the constants  $a$  and  $n$  describe the magnitude and slope of the continuum process. In the Breit-Wigner function for the resonance amplitude,  $M$ ,  $\Gamma$ , and  $\Gamma_{e^+e^-}$  are the mass, the total width, and the particle width to  $e^+e^-$  final state of the resonance  $R$ . In case of the  $\eta'\phi$  final state, the phase space factor is  $PS(\sqrt{s}) = [q(\sqrt{s})]^3/s$ , where  $q(\sqrt{s})$  is the momentum of  $\eta'$  or  $\phi$ . The following study focused on the optimization of statistical uncertainty. The values of the key parameter for the numerical calculations presented in the following sections are summarized in Table I. In the fitting procedure,  $\mathcal{B}$  and  $\phi$  are defined as two free parameters. The maximization of the likelihood function  $LF$  presented in Eq. (II.1) yields the optimal estimate for  $\mathcal{B}$ .

TABLE I. Values of key parameters for the numerical calculation. The quantities with  $\star$  are set as free parameters, and the others are fixed for the corresponding study.

Parameter	$\psi(3770) \rightarrow \text{non-}D\bar{D}$	$\Upsilon(4S) \rightarrow \text{non-}B\bar{B}$
$M$ (GeV/ $c^2$ )	3.7736 [2]	10.58 [2]
$\Gamma_{e^+e^-}$ (keV)	0.26 [2]	0.28 [2]
$\Gamma$ (MeV)	27.2 [2]	20.5 [2]
$\star\mathcal{B}$	free	free
$\star\phi$	free	free
$\epsilon$	10% [16–20]	15% [16–20]
$a$	1.82 [16–20]	$3.2 \times 10^{-2.5}$ [16–20]
$n$	5.82 [16–20]	3.00 [16–20]

In the following analysis, we assume that the value of  $\mathcal{B}$  is known. Under this assumption, we aim to address the questions posed at the end of Sec. I. However, upon further reflection on the first two questions, we notice that they are interconnected. Specifically, the optimal number of energy points depends on their distribution, and *vice versa*. To resolve this dilemma, we begin with a simple distribution to determine the optimal number of energy points, allowing us to finalize the total number of energy points needed.

## B. Two-parameter fit

We take  $N_{pt} = 100$  energy points and  $N_{br} = 300$  branching fractions as a tentative beginning. The values of energies and branching fractions are calculated via

$$E_{c.m.}^i = E_{c.m.}^0 + (i - 1) \times \delta E_{c.m.} \quad (i = 1, 2, \dots, N_{pt}), \quad (\text{II.6})$$

$$\mathcal{B}_j = \mathcal{B}_0 + (j - 1) \times \delta\mathcal{B} \quad (j = 1, 2, \dots, N_{br}), \quad (\text{II.7})$$

where  $E_{c.m.}^0 = 3.74$  GeV,  $\mathcal{B}_0 = 1 \times 10^{-6}$ ,  $E_{c.m.}^f = 3.80$  GeV, and  $\mathcal{B}_f = 1 \times 10^{-3}$  for  $\psi(3770)$  decays, and  $E_0 = 10.56$  GeV,  $\mathcal{B}_0 = 1 \times 10^{-9}$ ,  $E_f = 10.60$  GeV, and  $\mathcal{B}_f = 1 \times 10^{-6}$  for  $\Upsilon(4S)$  decays. The energy interval and branching fraction interval are calculated with  $\delta E_{c.m.} = (E_{c.m.}^f - E_{c.m.}^0)/N_{pt}$  and  $\delta\mathcal{B} = (\mathcal{B}_f - \mathcal{B}_0)/N_{br}$ .

To reduce the statistical fluctuation, sampling is repeated  $N_{\text{samp}} = 200$  times for each scheme of an  $E_{c.m.}^i$  and  $\mathcal{B}$  combination. The general flow chart of sampling and fitting is presented in Fig. 1. We obtain the mean value of  $\mathcal{B}_k^{ij}$  and its error  $\sigma(\mathcal{B}_k^{ij})$  from fitting to the  $k$ -th sample. The average value of  $\mathcal{B}$  and the corresponding uncertainty from fitting to the 200 samples are calculated via [22]

$$\bar{B}^{ij} = \frac{1}{N_{\text{samp}}} \sum_{k=1}^{N_{\text{samp}}} \mathcal{B}_k^{ij}, \quad \sigma(\bar{B}^{ij}) = \frac{1}{N_{\text{samp}}} \sum_{k=1}^{N_{\text{samp}}} \sigma(\mathcal{B}_k^{ij}). \quad (\text{II.8})$$

The average relative uncertainty is calculated via

$$\sigma(\mathcal{B}) = \sigma(\bar{B}^{ij})/\bar{B}^{ij}. \quad (\text{II.9})$$

Here, it should be noted that  $ij$  denotes a specific scheme of an  $E_{\text{c.m.}}^i$  and  $\mathcal{B}$  combination. Additionally,  $k$  represents the  $k$ -th sampling time.  $\bar{B}^{ij}$  and  $E(\bar{B}^{ij})$  represent the average value and the error of the branching fraction from the fit, respectively. Without the special declaration, the meaning of the average defined by Eqs. (II.8) and (II.9) is kept in the study follows.

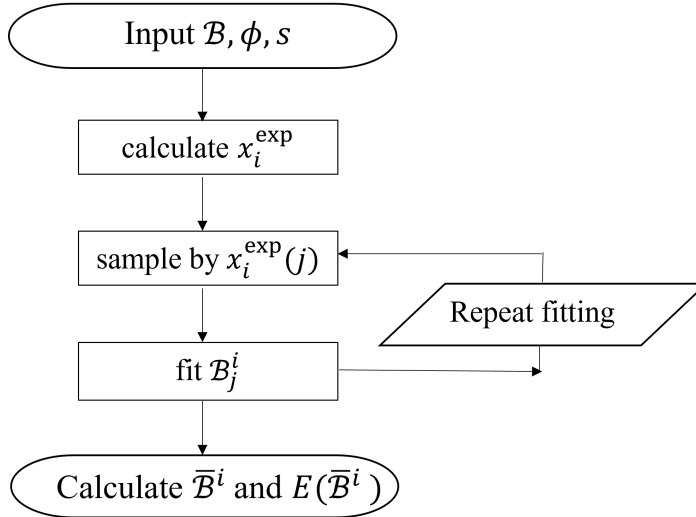


FIG. 1. Flow chart of the sampling, where  $ij$  ( $i = 1, 2, \dots, N_{\text{pt}}; j = 1, 2, \dots, N_{\text{br}}$ ) denotes a specific scheme of an  $E_{\text{c.m.}}^i$  and  $\mathcal{B}$  combination, and  $k$  ( $k = 1, 2, \dots, N_{\text{samp}}$ ) represents the  $k$ -th sampling time.

According to the available data at the BESIII experiment and future data acquisition strategies of the Belle II experiment, the integrated luminosities of the data we used are  $20 \text{ fb}^{-1}$  at  $\sqrt{s} = 3.773 \text{ GeV}$  and  $50 \text{ ab}^{-1}$  at  $\sqrt{s} = 10.58 \text{ GeV}$ , respectively.  $\mathcal{B}$  and  $\phi$  as free parameters in the fits, and we obtain the results for each  $30^\circ$  variations in the phase angle, as presented in Fig. 2 for  $\psi(3770)$  decays and Fig. 3 for  $\Upsilon(4S)$  decays. The colors represent the  $\sigma(\mathcal{B})$  for each energy point and branching fraction combination at the corresponding phase angle  $\phi$ .

### III. FISHER INFORMATION

In mathematical statistics, Fisher information quantifies the amount of information that a random variable  $X$  carries about a known parameter  $\theta$  [21]. In the context of our study, Fisher information is employed to estimate the parameter  $\theta = (\mathcal{B}, \phi)$  based on the observed event numbers  $\mathbf{x} = (x_1, x_2)$  as described in Sec. II A.

According to the previous Eq. II.1, the score function is constructed as

$$s(\theta, \mathbf{x}) = \frac{\partial[\log LF(\mathbf{x}; \mathcal{B}, \phi)]}{\partial \theta}, \quad (\text{III.1})$$

and the Fisher information matrix is defined as the covariance matrix of the score function. Concretely,

$$i(\theta) = E_\theta(s(\theta, \mathbf{x})s(\theta, \mathbf{x})^T). \quad (\text{III.2})$$

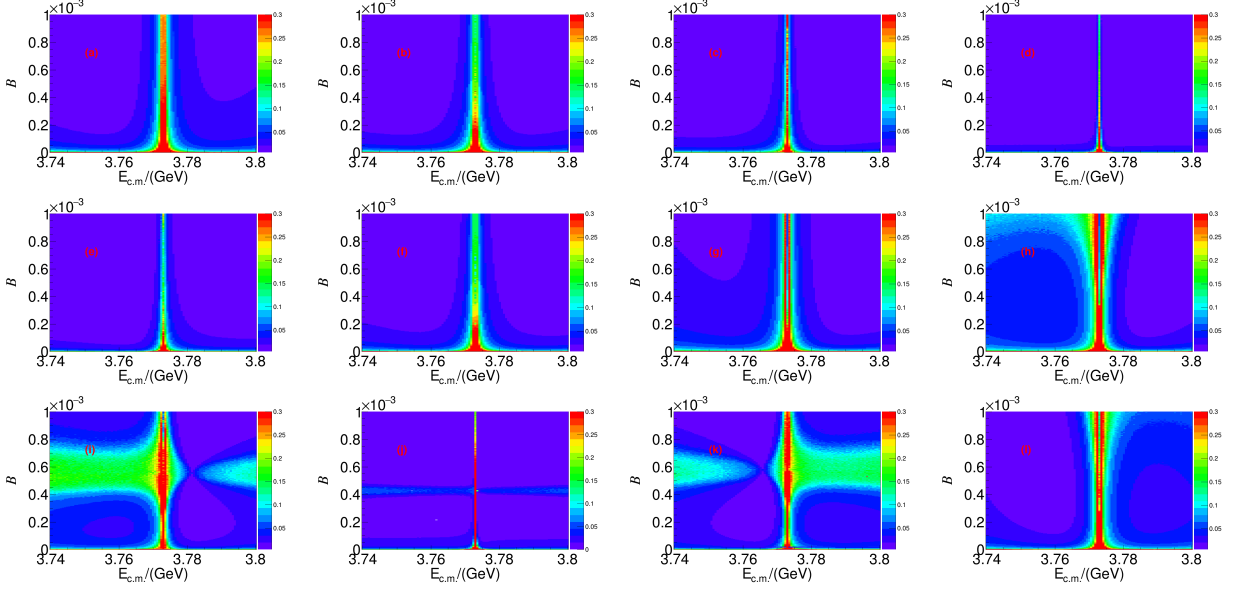


FIG. 2. The distributions of  $\sigma(\mathcal{B})$  along with  $E_{c.m.}^i$  and branching fraction for  $\psi(3770) \rightarrow \text{non-}D\bar{D}$  decays with different phase angle  $\phi$ : (a)  $0^\circ$ , (b)  $30^\circ$ , (c)  $60^\circ$ , (d)  $90^\circ$ , (e)  $120^\circ$ , (f)  $150^\circ$ , (g)  $180^\circ$ , (h)  $210^\circ$ , (i)  $240^\circ$ , (j)  $270^\circ$ , (k)  $300^\circ$ , and (l)  $330^\circ$ .

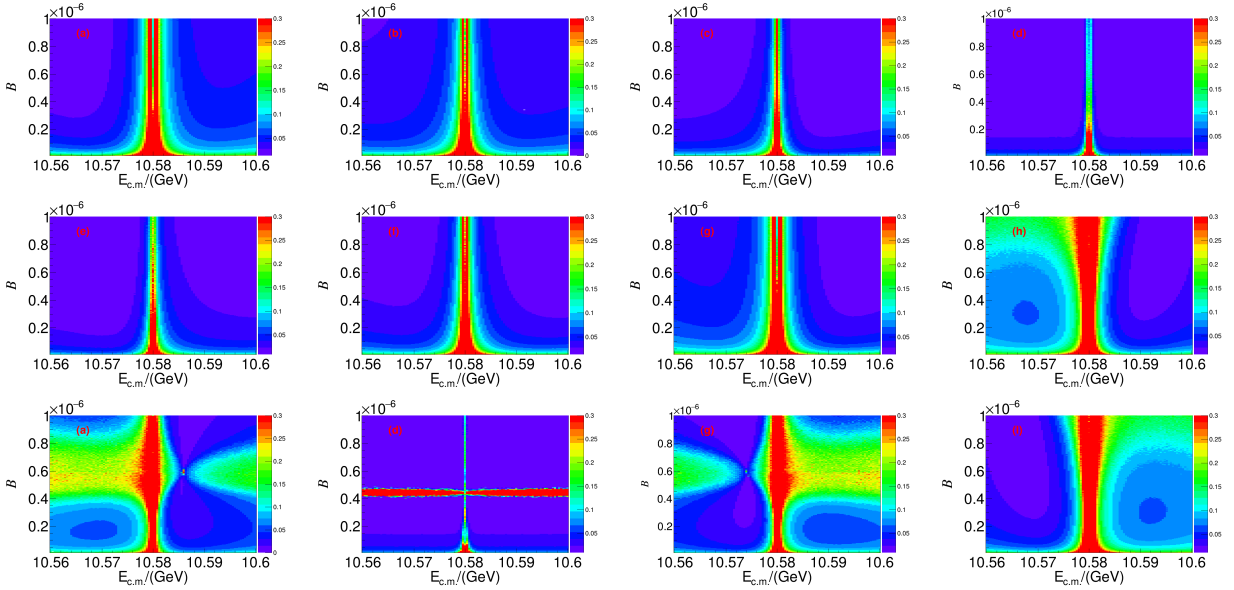


FIG. 3. The distributions of  $\sigma(\mathcal{B})$  along with  $E_{c.m.}^i$  and branching fraction for  $\Upsilon(4S) \rightarrow \text{non-}B\bar{B}$  decays with different phase angle  $\phi$ : (a)  $0^\circ$ , (b)  $30^\circ$ , (c)  $60^\circ$ , (d)  $90^\circ$ , (e)  $120^\circ$ , (f)  $150^\circ$ , (g)  $180^\circ$ , (h)  $210^\circ$ , (i)  $240^\circ$ , (j)  $270^\circ$ , (k)  $300^\circ$ , and (l)  $330^\circ$ .

where  $E_\theta$  represents the expected value of the outer product of the score function  $s(\theta, \mathbf{x})s(\theta, \mathbf{x})^T$  given the parameter  $\theta$ . When considering  $\mathcal{B}$  and  $\phi$  as two free parameters, the Fisher information matrix of  $\theta = (\mathcal{B}, \phi)$  is a  $2 \times 2$  matrix, and the elements of the Fisher matrix are

$$\begin{aligned} i_{11} &= \int \int \left( \frac{\partial[\log LF(\mathbf{x}; \mathcal{B}, \phi)]}{\partial \mathcal{B}} \right)^2 \cdot LF(\mathbf{x}; \mathcal{B}, \phi) d^2 \mathbf{x}, \\ i_{12} = i_{21} &= \int \int \left( \frac{\partial[\log LF(\mathbf{x}; \mathcal{B}, \phi)]}{\partial \mathcal{B}} \frac{\partial[\log LF(\mathbf{x}; \mathcal{B}, \phi)]}{\partial \phi} \right) \cdot LF(\mathbf{x}; \mathcal{B}, \phi) d^2 \mathbf{x}, \\ i_{22} &= \int \int \left( \frac{\partial[\log LF(\mathbf{x}; \mathcal{B}, \phi)]}{\partial \phi} \right)^2 \cdot LF(\mathbf{x}; \mathcal{B}, \phi) d^2 \mathbf{x}, \end{aligned}$$

where indices 1 and 2 indicate  $\mathcal{B}$  and  $\phi$ , respectively. Inverting the  $2 \times 2$  matrix yields the asymptotic covariance matrix

$$\begin{bmatrix} (i_{11} - \frac{i_{12}^2}{i_{22}})^{-1} & (\frac{i_{11}i_{22}}{i_{12}} - i_{12})^{-1} \\ (\frac{i_{11}i_{22}}{i_{12}} - i_{12})^{-1} & (i_{22} - \frac{i_{12}^2}{i_{11}})^{-1} \end{bmatrix}. \quad (\text{III.3})$$

Hence, the variance of the branching fraction can be determined as,

$$\left( i_{11} - \frac{i_{12}^2}{i_{22}} \right)^{-1} = \frac{2(D\phi_1^2 \cdot (1 + 2x_1^{\text{exp}})(x_2^{\text{exp}})^2 + D\phi_2^2 \cdot (1 + 2x_2^{\text{exp}})(x_1^{\text{exp}})^2)}{(DB_2 \cdot D\phi_1 - DB_1 \cdot D\phi_2)^2 (1 + 2x_1^{\text{exp}})(1 + 2x_2^{\text{exp}})}, \quad (\text{III.4})$$

Where  $x_1^{\text{exp}}$  and  $x_2^{\text{exp}}$  are the expected events at energy points  $E_{\text{c.m.}}^i$  and the resonance, respectively.  $DB_i$  and  $D\phi_i$  denote  $\partial x_i^{\text{exp}}/\partial \mathcal{B}$  and  $\partial x_i^{\text{exp}}/\partial \phi$ , respectively. As in the Sec. II, we present the  $\sigma(\mathcal{B})$  using Fisher information. The same phase  $\phi$  distributions are shown in Figs. 4 and 5. The results are consistent with the methodology employed in the MC simulation.

#### IV. DATA TAKING ENERGY POINTS

Drawing from previous studies, a critical question emerges: Where should the optimal energy point be? In addressing this inquiry, Ref. [15] indicates that the relative phase  $\phi$  is approximately  $270^\circ$ . Accordingly, Figs. 6 and 7 present the fitting results for  $\phi$  ranging from  $240^\circ$  to  $300^\circ$  in  $10^\circ$  increments. The red line in each plot represents the optimal energy point corresponding to the best precision of  $\sigma(\mathcal{B})$ , as determined by the branching fraction. According to the accumulations of the optimal  $E_{\text{c.m.}}$  illustrated in Fig. 8, the optimal energy points for  $\psi(3770) \rightarrow \text{non-}D\bar{D}$  decays are 3.769 GeV and 3.781 GeV, while those for  $\Upsilon(4S) \rightarrow \text{non-}B\bar{B}$  decays are 10.574 GeV and 10.585 GeV. We should note that the optimal energies will differ if the phase  $\phi$  is in different ranges.

#### V. INTEGRATED LUMINOSITY AND UNCERTAINTY

##### A. Integrated luminosity requirements for data taking strategy

The last question is the relationship between the integrated luminosity and the precision of branching fraction measurements. For the fitting procedure involving branching fractions

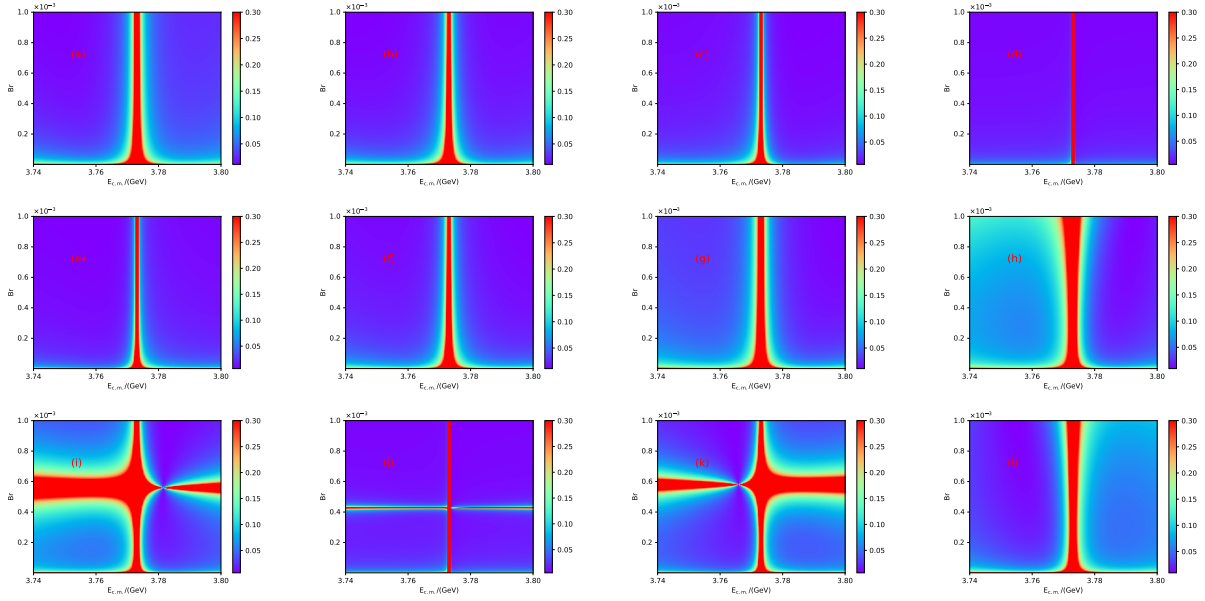


FIG. 4. The distributions of  $\sigma(\mathcal{B})$  along with  $E_{c.m.}^i$  and branching fraction obtained by Fisher information for  $\psi(3770) \rightarrow \text{non-}D\bar{D}$  decays with different phase angle  $\phi$ : (a)  $0^\circ$ , (b)  $30^\circ$ , (c)  $60^\circ$ , (d)  $90^\circ$ , (e)  $120^\circ$ , (f)  $150^\circ$ , (g)  $180^\circ$ , (h)  $210^\circ$ , (i)  $240^\circ$ , (j)  $270^\circ$ , (k)  $300^\circ$ , and (l)  $330^\circ$ .

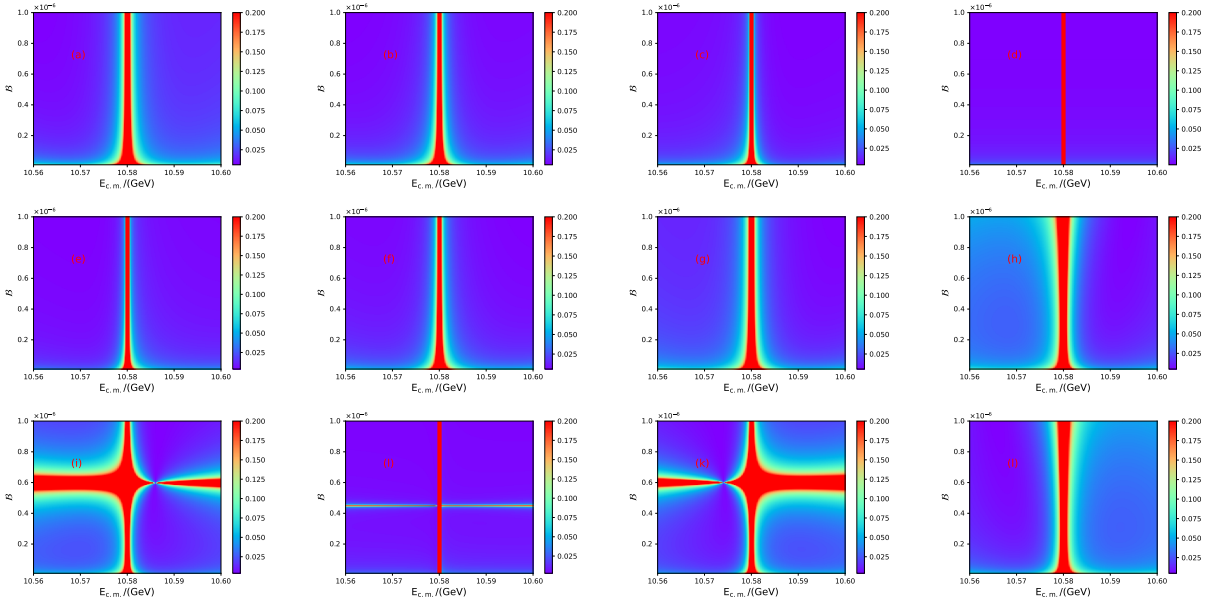


FIG. 5. The distributions of  $\sigma(\mathcal{B})$  along with  $E_{c.m.}^i$  and branching fraction obtained by Fisher information for  $\Upsilon(4S) \rightarrow \text{non-}B\bar{B}$  decays with different phase angle  $\phi$ : (a)  $0^\circ$ , (b)  $30^\circ$ , (c)  $60^\circ$ , (d)  $90^\circ$ , (e)  $120^\circ$ , (f)  $150^\circ$ , (g)  $180^\circ$ , (h)  $210^\circ$ , (i)  $240^\circ$ , (j)  $270^\circ$ , (k)  $300^\circ$ , and (l)  $330^\circ$ .



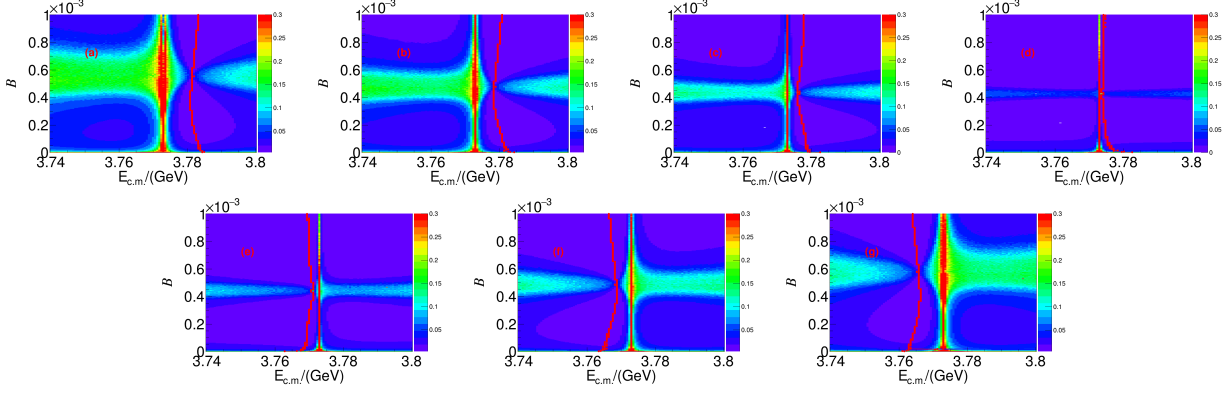


FIG. 6. The distributions of  $\sigma(\mathcal{B})$  along with  $E_{c.m.}^i$  and branching fraction for  $\psi(3770) \rightarrow \text{non-}D\bar{D}$  decays from specific phase angle  $\phi$ : (a)  $240^\circ$ , (b)  $250^\circ$ , (c)  $260^\circ$ , (d)  $270^\circ$ , (e)  $280^\circ$ , (f)  $290^\circ$ , and (g)  $300^\circ$ . The red lines show the best precision of  $\sigma(\mathcal{B})$  versus the branching ratio  $\mathcal{B}$ .

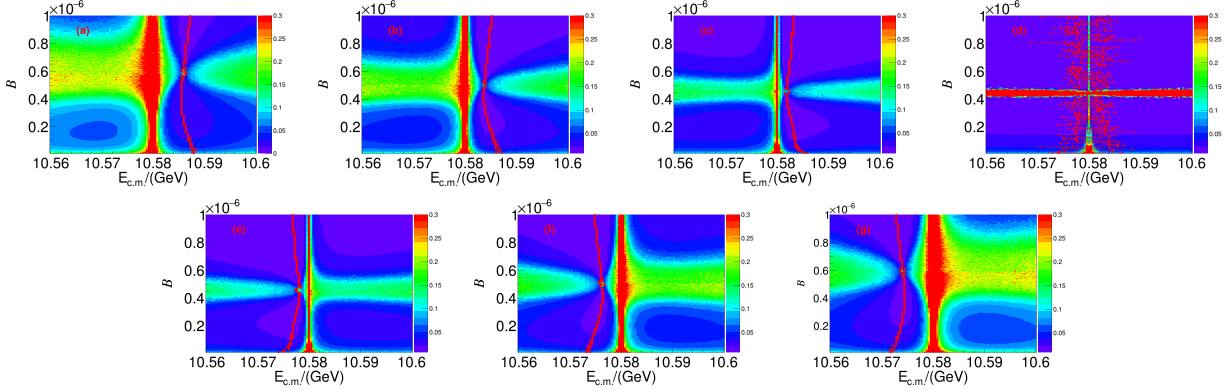


FIG. 7. The distributions of  $\sigma(\mathcal{B})$  along with  $E_{c.m.}^i$  and branching fraction for  $\Upsilon(4S) \rightarrow \text{non-}B\bar{B}$  decays from specific phase angle  $\phi$ : (a)  $240^\circ$ , (b)  $250^\circ$ , (c)  $260^\circ$ , (d)  $270^\circ$ , (e)  $280^\circ$ , (f)  $290^\circ$ , and (g)  $300^\circ$ . The red lines show the best precision of  $\sigma(\mathcal{B})$  versus the branching ratio  $\mathcal{B}$ .

that span several orders of magnitude, we assume an equal allocation of integrated luminosity between the low-energy ( $L_{\text{low}}$ ) and high-energy ( $L_{\text{high}}$ ) data acquisition points. The results of the integrated luminosity optimization for  $\psi(3770)$  are shown in Fig. 9, where seven curves represent different relative phases ( $\phi = 240^\circ, 250^\circ, 260^\circ, 270^\circ, 280^\circ, 290^\circ, 300^\circ$ ). Similarly, Fig. 10 illustrates a corresponding integrated luminosity optimization scheme for the  $\Upsilon(4S)$ . Table II summarizes the integrated luminosity requirements for an effective data acquisition strategy aimed at achieving a projected 10% precision of  $\sigma(\mathcal{B})$  at both energy points. The results indicate that a minimum integrated luminosity of 500 pb is required for the  $\psi(3770)$  decays, while 200 fb is necessary for the  $\Upsilon(4S)$  decays.

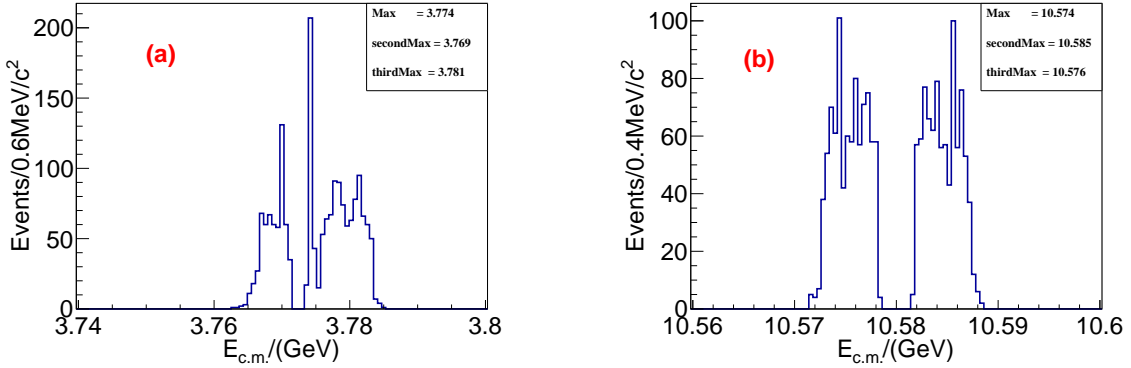


FIG. 8. The accumulation of optimal energy positions for  $\phi$  from  $240^\circ$  to  $300^\circ$  for (a)  $\psi(3770)$  decays and (b)  $\Upsilon(4S)$  decays.

TABLE II. The relationship between integrated luminosity and  $\mathcal{B}$  with  $\sigma(\mathcal{B})$  fixed to 10%.

$\mathcal{B}$	$\psi(3770) \rightarrow \text{non-}D\bar{D}$	$\mathcal{B}$	$\Upsilon(4S) \rightarrow \text{non-}B\bar{B}$
$1 \times 10^{-3}$	500 pb	$1 \times 10^{-6}$	200 fb
$1 \times 10^{-4}$	800 pb	$1 \times 10^{-7}$	800 fb
$1 \times 10^{-5}$	3 fb	$1 \times 10^{-8}$	5 ab
$1 \times 10^{-6}$	14 fb		

## B. Optimization of integrated luminosity allocation

Based on the findings presented in Sec. V A, we initially assumed an integrated luminosity ratio of  $L_{\text{low}} : L_{\text{high}} = 1 : 1$  without considering the effects of different integrated luminosities at different energy points. To achieve optimal precision in the branching fraction measurements, we vary the parameter  $X_i \equiv L_{\text{low}} / (L_{\text{low}} + L_{\text{high}})$  to determine the corresponding  $\sigma(\mathcal{B})$ . The optimized  $X_i$  values for both energy points related to  $\psi(3770)$  are shown in Fig. 11. Figure 12 illustrates a similar integrated luminosity optimization scheme for the  $\Upsilon(4S)$ . From the curves in Figs. 11 and 12, we find that the minimum value of  $\sigma(\mathcal{B})$  occurs at  $X_i = 0.3$  for  $\psi(3770) \rightarrow \text{non-}D\bar{D}$  decays and  $X_i = 0.5$  for  $\Upsilon(4S) \rightarrow \text{non-}B\bar{B}$  decays, which correspond to integrated luminosity ratios of  $L_{\text{low}} : L_{\text{high}} = 3 : 7$  and  $1 : 1$ , respectively.

## VI. DISCUSSION

The minor deviations, either higher or lower than the continuum cross sections observed in Refs. [3, 6–9], may have indicated nonzero  $\psi(3770)$  decays into light hadron final states, and more data are needed to confirm the observations. In the BESIII experiment, the peak luminosity is approximately  $1 \times 10^{33} \text{ cm}^{-2}\text{s}^{-1}$  at  $\sqrt{s} = 3.773 \text{ GeV}$ . A data acquisition period of 12 days is expected to be sufficient to achieve a projected precision of 10% in the measurements of the  $\psi(3770) \rightarrow \text{non-}D\bar{D}$  branching fraction.

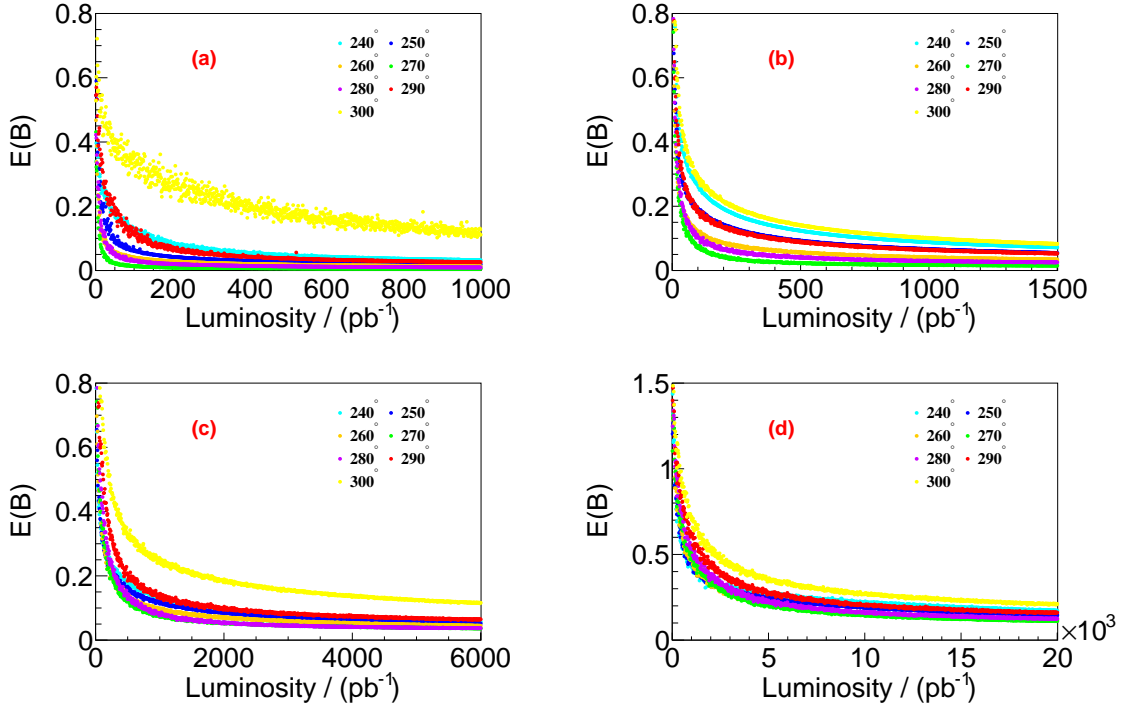


FIG. 9. The distributions of  $\sigma(\mathcal{B})$  along with the integrated luminosity of data sample for  $\psi(3770) \rightarrow$  non- $D\bar{D}$  decays with a branching fraction of (a)  $1 \times 10^{-3}$ , (b)  $1 \times 10^{-4}$ , (c)  $1 \times 10^{-5}$ , and (d)  $1 \times 10^{-6}$ .

In June 2022, SuperKEKB, the asymmetric energy accelerator that provides  $e^+e^-$  collisions inside the Belle II detector, achieved a new luminosity record of  $4.7 \times 10^{34} \text{ cm}^{-2}\text{s}^{-1}$  and recorded  $15 \text{ fb}^{-1}$  data per week. SuperKEKB aims to achieve a luminosity higher than  $1 \times 10^{35} \text{ cm}^{-2}\text{s}^{-1}$  in the near future. This accomplishment enables measurements with a branching fraction uncertainty of 10% to be completed within two months. Supposing this larger data sample is collected slightly above the  $\Upsilon(4S)$  peak, it will allow for the direct measurement of the  $B^+$  to  $B^0$  production ratio at a new energy point, and thereby enhance the constraints on the energy dependence of this ratio. Additionally, the study will explore potential molecular states near the  $B^*\bar{B}^*$  or  $B\bar{B}^*$  threshold, search for inelastic channels such as  $\pi^+\pi^-\Upsilon(1S, 2S)$  and  $\eta h_b(1P)$ , and investigate the violation of the isospin symmetry, among other topics.

## VII. SUMMARY

In conclusion, we have employed MC simulation methodology and Fisher information to investigate various data taking strategies for precisely measuring the branching fractions of  $\psi(3770) \rightarrow$  non- $D\bar{D}$  and  $\Upsilon(4S) \rightarrow$  non- $B\bar{B}$  decays. This analysis has enabled us to identify an optimal measurement scheme. In response to the questions outlined in Sec. I, we present the following answers:

- The optimal positions for data taking are located at 3.769 GeV and 3.781 GeV for

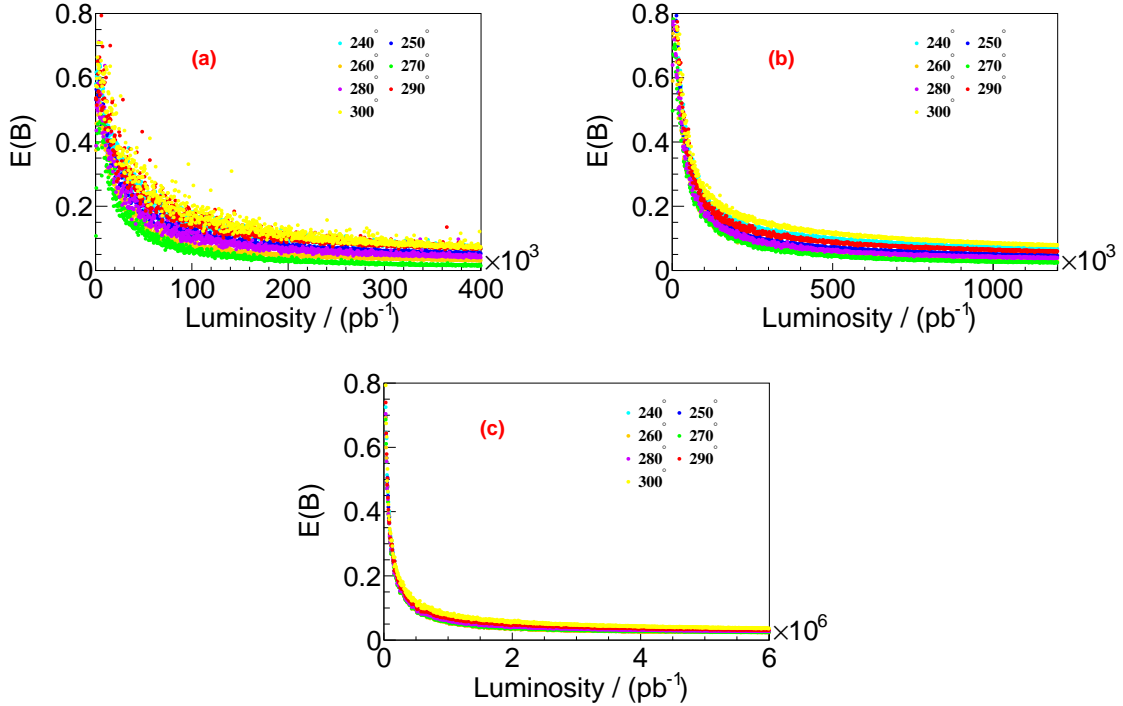


FIG. 10. The distributions of  $\sigma(\mathcal{B})$  along with the integrated luminosity of data sample for  $\Upsilon(4S) \rightarrow$  non- $B\bar{B}$  decays with a branching fraction of (a)  $1 \times 10^{-6}$ , (b)  $1 \times 10^{-7}$ , and (c)  $1 \times 10^{-8}$ .

$\psi(3770) \rightarrow$  non- $D\bar{D}$  decays, and 10.574 GeV and 10.585 GeV for  $\Upsilon(4S) \rightarrow$  non- $B\bar{B}$  decays;

- Two optimal energy points are sufficient to achieve a small uncertainty in the measurements of the branching fractions;
- To achieve an expected precision of 10% in branching fraction measurements, minimum integrated luminosities of 500 pb and 200 fb with recommended allocation of  $L_{\text{low}} : L_{\text{high}} = 3 : 7$  and  $1 : 1$  are required for  $\psi(3770) \rightarrow$  non- $D\bar{D}$  and  $\Upsilon(4S) \rightarrow$  non- $B\bar{B}$  decays, respectively.

We emphasize that the above conclusions are for an expected phase angle  $\phi$  close to  $270^\circ$ . The outcomes could vary significantly if the phase angle deviates substantially from this range. Nonetheless, the MC simulation and Fisher information techniques discussed in this article can be applied similarly across all scenarios. This approach allows for determining optimal energies and integrated luminosity allocations in various contexts.

### VIII. ACKNOWLEDGMENTS

This work is supported by the National Key R&D Program of China under Contract Nos. 2022YFA1601903 and 2020YFA0406300, and National Natural Science Foundation of China

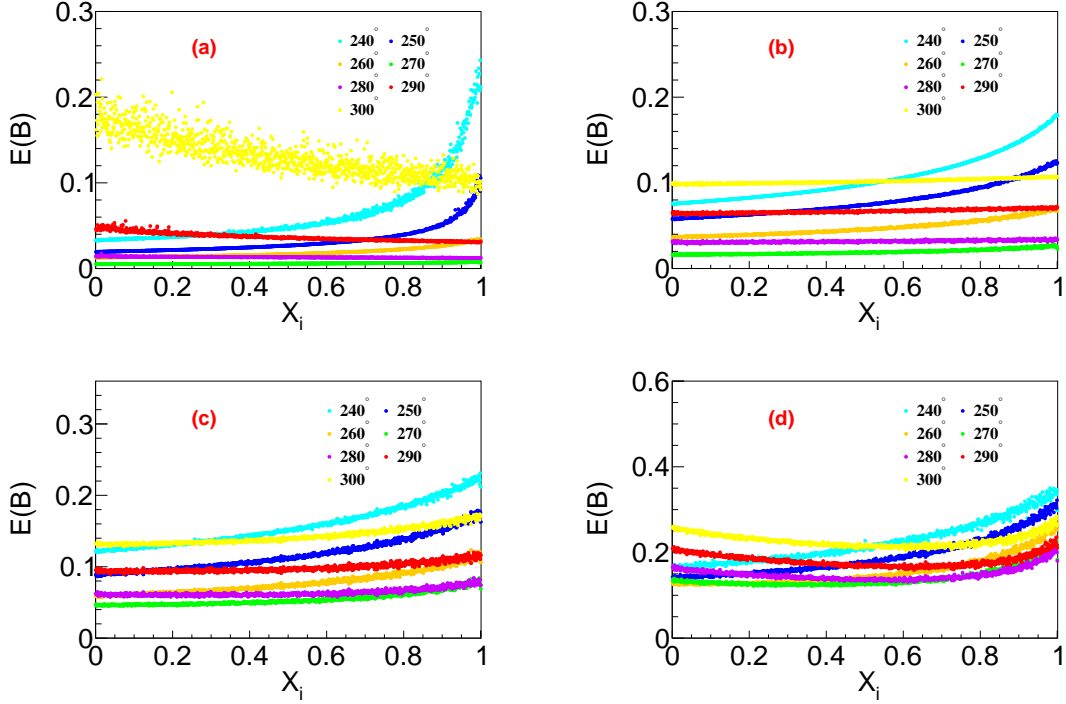


FIG. 11. The distributions of  $\sigma(\mathcal{B})$  along with the integrated luminosity allocation ratio  $X_i$  for  $\psi(3770) \rightarrow \text{non-}D\bar{D}$  decays with a branching fraction of (a)  $1 \times 10^{-3}$ , (b)  $1 \times 10^{-4}$ , (c)  $1 \times 10^{-5}$ , and (d)  $1 \times 10^{-6}$ . The total luminosities and  $\mathcal{B}$ s are fixed according to Table II.

under Contract Nos. 12175041, 12335004, and 12361141819.

- 
- [1] M. Ardu and G. Pezzullo, Phys. Lett. B **5**, 165 (1963); G. Zweig, CERN-preprint Report Nos. CERN-TH-401, 402, 412, 1964; J. Iizuka, Prog. Theor. Phys. Suppl. **37**, 21 (1996).
  - [2] S. Navas *et al.* [Particle Data Group], Phys. Rev. D **110**, 030001 (2024).
  - [3] M. Ablikim *et al.* (BESIII Collaboration), Phys. Rev. D **104**, 112009 (2021).
  - [4] M. Ablikim *et al.* (BESIII Collaboration), Phys. Lett. B **735**, 101 (2014).
  - [5] M. Ablikim *et al.* (BESIII Collaboration), Phys. Rev. D **90**, 032007 (2014).
  - [6] M. Ablikim *et al.* (BESIII Collaboration), Phys. Rev. D **87**, 112011 (2013).
  - [7] M. Ablikim *et al.* (BESIII Collaboration), Phys. Lett. B **650**, 111 (2007).
  - [8] G. S. Huang *et al.* (CLEO Collaboration), Phys. Rev. Lett. **96**, 032003 (2006).
  - [9] G. S. Adams *et al.* (CLEO Collaboration), Phys. Rev. D **73**, 012002 (2006).
  - [10] C. P. Shen *et al.* (Belle Collaboration), Phys. Rev. D **88**, 052019 (2013).
  - [11] K. Belous *et al.* (Belle Collaboration), Phys. Lett. B **681**, 400 (2009).
  - [12] Y. P. Guo and C. Z. Yuan, Phys. Rev. D **105**, 114001 (2022).
  - [13] M. Ablikim *et al.* (BESIII collaboration), Chin. Phys. C **44**, 04001 (2020).
  - [14] E. Kou *et al.* (Belle II Collaboration), Prog. Theor. Exp. Phys. **2019**, 123C01 (2019).

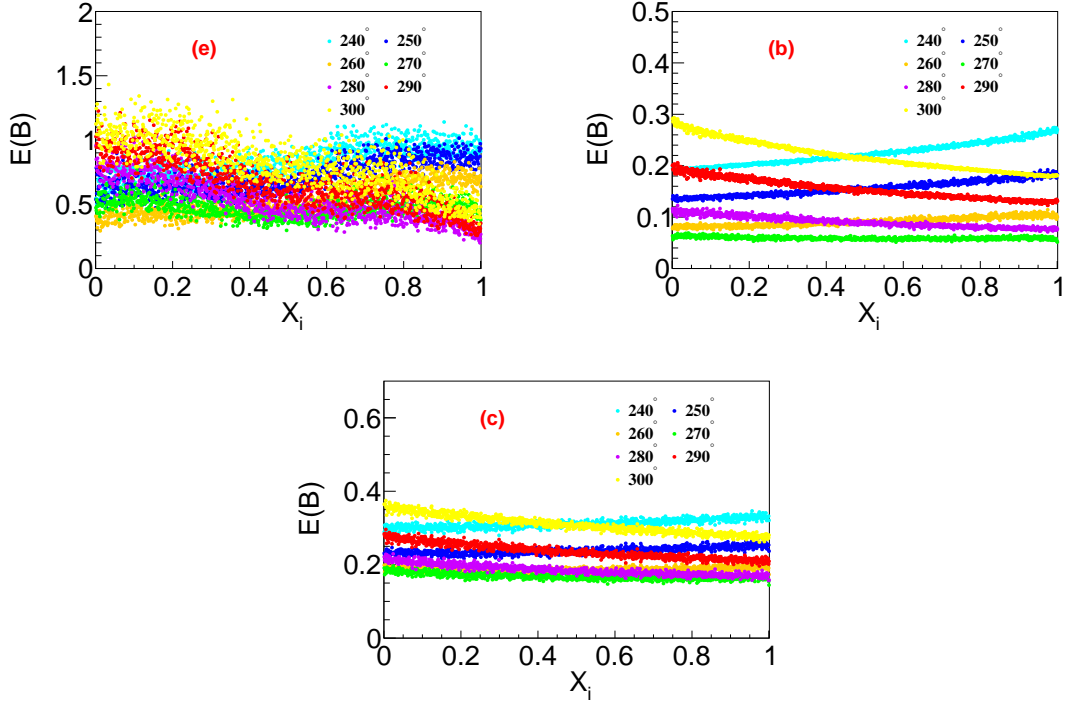


FIG. 12. The distributions of  $\sigma(\mathcal{B})$  along with the integrated luminosity allocation ratio  $X_i$  for  $\Upsilon(4S) \rightarrow \text{non-}B\bar{B}$  decays with a branching fraction of (a)  $1 \times 10^{-6}$ , (b)  $1 \times 10^{-7}$ , and (c)  $1 \times 10^{-8}$ . The total integrated luminosities and  $\mathcal{B}$ s are fixed according to Table II.

- [15] P. Wang, C. Z. Yuan and X. H. Mo, Phys. Rev. D **69**, 057501 (2004).
- [16] B. Aubert *et al.* (BaBar Collaboration), Phys. Rev. D **78**, 071103 (2008).
- [17] C. P. Shen *et al.* (Belle Collaboration), Phys. Rev. D **88**, 052019 (2013).
- [18] M. Ablikim *et al.* (BES III Collaboration), Phys. Rev. D **73**, 012002 (2006).
- [19] M. Ablikim *et al.* (BES III Collaboration), Phys. Rev. D **108**, 052015 (2023)
- [20] M. Ablikim *et al.* (BES III Collaboration), Phys. Rev. Lett. **132**, 131901 (2024).
- [21] J. Liu, H. Yuan and X. M. Wang, J. Phys. A: Math. Theor. **53**, 023001 (2020)
- [22] S. Brandt, Data Analysis, third ed., Springer, Verlag, 1999.